



Soil Moisture Sensor Network Design for Hydrological Applications

Lu Zhuo^{1,2}, Qiang Dai^{2,3*}, Binru Zhao⁴, Dawei Han⁵

¹Department of Civil and Structural Engineering, University of Sheffield, Sheffield, UK

²Key Laboratory of VGE of Ministry of Education, Nanjing Normal University, Nanjing, China

³Jiangsu Center for Collaborative Innovation in Geographical Information Resource Development and Application, Nanjing, China

⁴College of Water Conservancy and Hydropower Engineering, Hohai University, Nanjing, China

⁵WEMRC, Department of Civil Engineering, University of Bristol, Bristol, UK

*Correspondence: qd_gis@163.com

Abstract

Soil moisture plays an important role in the partitioning of rainfall into evapotranspiration, infiltration and runoff, hence a vital state variable in the hydrological modelling. However, due to the heterogeneity of soil moisture in space most existing in-situ observation networks rarely provide sufficient coverage to capture the catchment-scale soil moisture variations. Clearly, there is a need to develop a systematic approach for soil moisture network design, so that with the minimal number of sensors the **catchment spatial soil moisture information** could be captured accurately. In this study, a simple and low-data requirement method is proposed. It is based on the Principal Component Analysis (PCA) and Elbow curve for the determination of the optimal number of soil moisture sensors; and *K*-means Cluster Analysis (CA) and a selection of statistical criteria for the identification of the sensor placements. Furthermore, the long-term (10-year) **soil moisture datasets** estimated through the advanced Weather Research and Forecasting (WRF) model are used as the network design inputs. In the case of the Emilia Romagna catchment, the results show the proposed network is very efficient in estimating the **catchment-scale soil moisture** (i.e., with *NSE* and *r* at 0.995 and 0.999, respectively for the areal mean estimation; and 0.973 and 0.990, respectively for the areal standard deviation estimation). To retain 90% variance, a total of 50 sensors in a 22,124 km² catchment is needed,



29 which in comparison with the original number of WRF grids (828 grids), the designed network
30 requires significantly fewer sensors. However, refinements and investigations are needed to
31 further improve the design scheme which are also discussed in the paper.

32 **Keywords:** Soil moisture network design, Principal Component Analysis (PCA), *K*-means
33 Cluster Analysis (CA), Weather Research and Forecasting (WRF) Model, Optimising,
34 Numerical Weather Prediction (NWP) model.

35

36

37 1. Introduction

38 Soil moisture is at the heart of the Earth system and it plays an important role in the exchanges
39 of water and energy at the land surface (Dorigo et al., 2017;Robock et al., 2000;Crow et al., 2018).
40 In hydrology, soil moisture is the key component for the partitioning of rainfall into
41 evapotranspiration, infiltration and runoff (Vereecken et al., 2008;Brocca et al., 2017;Rajib et al.,
42 2016;Fuamba et al., 2019). In particular, the antecedent soil moisture condition of a catchment is
43 among one of the most important factors for flood triggering (Uber et al., 2018;Zhuo and Han,
44 2017). For hydrological modelling, soil moisture is a vital state variable. Especially, during
45 real-time flood forecasting, the accurate updating of the soil moisture state variable is a critical
46 step to reduce the accumulation of model errors (i.e., time drift problem) (Lopez et al.,
47 2016;Laiolo et al., 2016;Zwieback et al., 2019). Therefore, the intensive monitoring of catchment-
48 scale soil moisture content would benefit a number of hydrological applications.

49 In-situ soil moisture sensors (e.g., capacitance probe, and Time Domain Reflectometry), ~~as one~~
50 ~~of the oldest and most common methods used around the world,~~ can provide point-based soil
51 moisture measurements with relatively high accuracy in comparison with the modelling and
52 the remotely sensed approaches (Albergel et al., 2012). Therefore, they are a crucial source of
53 information for the hydrological research (Western et al., 2004;Brocca et al., 2017). However, due
54 to the heterogeneity of soil moisture in large space and the economic considerations, most



55 existing in-situ networks rarely provide sufficient coverage to capture the catchment soil
56 moisture variations (Chaney et al., 2015). In particular, in a number of cases, soil moisture
57 sensors are mainly installed close to the residential plain areas (e.g., due to easy accessibility
58 and maintenance reasons), and there is a lack of sensors installed in the complex topographic
59 areas ~~where they are really the most needed~~ (Zhuo et al., 2019b). Therefore, there is a need to
60 develop a systematic approach for the soil moisture network design, so that with the minimal
61 number of sensors the catchment-scale soil moisture information could be captured accurately.
62 However, to our knowledge, there is a lack of existing literature covering such a research area
63 particularly for the hydrological applications (Chaney et al., 2015), albeit numerous studies have
64 been carried out on the rain gauge network design ~~by the community~~ (Dai et al., 2017; Adhikary
65 et al., 2015; Pardo-Igúzquiza, 1998; Chen et al., 2008; Bayat et al., 2019).

66 Therefore, to address the aforementioned research gap, the aim of this paper is to propose a
67 ~~pioneer~~ soil moisture network design scheme for catchment-scale studies, based on a
68 combination of statistical approaches. In particular, the Principal Component Analysis (PCA)
69 and Elbow curve are adopted to determine the optimal number of soil moisture sensors within
70 a catchment, and *K*-means Cluster Analysis (CA) and a selection of statistical criteria are used
71 for the identification of the soil moisture sensor placements. Although the methodologies
72 themselves are not new, it is the first time they are applied for the soil moisture network design.
73 Furthermore, long-term (10-year) soil moisture datasets estimated through the advanced
74 Numerical Weather Prediction (NWP) Weather Research and Forecasting (WRF) model
75 (Skamarock et al., 2008) are used as the design inputs. WRF model has been applied in a wide
76 range of applications with good performances (Srivastava et al., 2015; Zaitchik et al., 2013; Zhuo et
77 al., 2019a; Stéfanon et al., 2014). Although WRF estimated soil moisture cannot represent the
78 ground truth, they are ideal datasets to provide catchment characteristics, such as land cover,
79 soil properties, topographies, which are the main drivers of local soil moisture heterogeneity



80 (Friesen et al., 2008). Therefore, such globally available datasets together with the proposed
81 statistical approaches would provide useful insights for the soil moisture network design
82 research (i.e., to minimise the redundancy of information, and improve accuracy), in particular,
83 for those currently ungauged catchments. In this study, the proposed method is implemented
84 in the Emilia Romagna region, northern Italy as a case study due to its high-exposure of flood
85 events.

86 The paper is organised as: the study area is introduced in Section 2; soil moisture network
87 design methodologies are described in Section 3; the results are presented in Section 4; and
88 discussions and conclusions are included in Section 5.

89 **2. Study Area**

90 In this study, the Emilia Romagna region (latitude 43°50'N–45°00'N; longitude 9°20'E–12°40'E)
91 is selected for the case study which is in Northern Italy (Figure 1). The region's total coverage
92 is approximately 22,124 km². It is surrounded by the Apennines to the south and the Adriatic
93 Sea to the east, with over half of the area as a plain agricultural zone (12,000 km²). The climate
94 condition is highly varied in the region which is largely influenced by the mountains and the
95 sea, with subcontinental in the Po Plain and hilly areas, and cool temperate in the mountain
96 range (Nistor, 2016). It has distinct wet and dry seasons (i.e. dry season between May and
97 October, and wet season between November and April) (Zhuo et al., 2019b). Based on the ESA
98 CCI land cover map (Bontemps et al., 2013), the region is mainly covered by Herbaceous (37%),
99 followed by Tree (22%), and Cropland (21%). The majority of the area is on the quaternary
100 alluvial deposits, which are characterised by a high degree of heterogeneity (Pistocchi et al.,
101 2015). The annual temperature ranges from 8.2 to 19.3°C; and the annual mean precipitation is
102 between 520 and 820 mm (Pistocchi et al., 2015).



103 For the soil moisture network in the region, currently, there is a total of 19 soil moisture sensors
104 installed (all located in the plain area); however only one of them can provide long-term
105 continuous soil moisture monitoring datasets. The network is managed by the Regional Agency
106 for Environmental Protection Emilia Romagna Region. Through further investigations, it has
107 been found, a number of the sensors have actually never provided proper soil moisture
108 measurements since the installation. For such a highly heterogeneous catchment, only one soil
109 moisture sensor at the plain area is clearly not sufficient for any catchment-scale applications.
110 Therefore, it is hoped the proposed soil moisture network design scheme could provide some
111 useful guidance to the local authority on an improved network in the future (i.e., a minimum
112 number of sensors for reduced installation and maintenance cost, but at the right locations).

113 **3. Methodologies**

114 **3.1 WRF Model**

115 The WRF model is a next-generation, non-hydrostatic mesoscale NWP system designed for
116 both atmospheric research and operational forecasting applications (Skamarock et al., 2005). The
117 model is capable of modelling a wide range of meteorological applications varying from tens
118 of metres to thousands of kilometres (NCAR, 2018). Apart from the WRF's aforementioned
119 advantage on including the catchment characteristics for the **soil moisture estimations**, it also
120 has other merits that make it an ideal tool for providing the distributed soil moisture information
121 for the network design. For instance, WRF model's spatial and temporal resolutions can be
122 changed depending on the input datasets to fit various application requirements, and a number
123 of globally-available data products can be selected to provide the necessary boundary and
124 initial conditions for running the model. Therefore, WRF is able to provide valuable
125 information for this study. Here WRF version 3.8 with the **ARW** dynamic core is used.

126 **3.1.1 Model Parameterization**



127 Apart from the atmospheric forcing, parameterization is also required to drive the WRF model.
128 In particular, the microphysics scheme is important in simulating accurate rainfall information
129 which in turn is significant for estimating the accurate soil moisture fluctuations. WRF V3.8
130 supports 23 microphysics options ranging from simple to more sophisticated mixed-phase
131 physical options. In this study, the WRF Single-Moment 6-class scheme is adopted which
132 considers ice, snow and graupel processes and is suitable for high-resolution applications (Zaidi
133 and Gisen, 2018). The physical options used in the WRF setup are Dudhia shortwave radiation
134 (Dudhia, 1989) and Rapid Radiative Transfer Model (RRTM) longwave radiation (Mlawer et
135 al., 1997). Cumulus parameterization is based on the Kain-Fritsch scheme (Kain, 2004b) which
136 is capable of representing sub-grid scale features of the updraft and rain processes, and such a
137 feature is useful for real-time modelling (Gilliland and Rowe, 2007). The surface layer
138 parameterization is based on the Revised fifth-generation Pennsylvania State University–
139 National Center for Atmospheric Research Mesoscale Model (MM5) Monin-Obukhov scheme
140 (Jiménez et al., 2012a). The planetary boundary layer is calculated based on the Yonsei
141 University scheme (Hong et al., 2006a). In WRF, its land surface model plays a vital role in
142 the integration of information generated through the surface layer scheme, the radiative forcing
143 from the radiation scheme, the precipitation forcing from the microphysics and convective
144 schemes, and the land surface conditions to simulate the water and energy fluxes (Ek et al.,
145 2003). In this study, the Noah Multiparameterization (Noah-MP) is chosen, because it has
146 shown more accurate soil moisture estimation performance than the other two main schemes
147 (Noah and CLM4) in other studies (Cai et al., 2014;Zhuo et al., 2019a). Table 1 shows the selected
148 WRF parameterization schemes. The static inputs (i.e., land use and soil texture) are chosen in
149 the WRF pre-processing package. Here, the land use categorisation is interpolated from the
150 MODIS 21-category data classified by the International Geosphere Biosphere Programme



151 (IGBP). The soil texture data are based on the Food and Agriculture Organization of the United
152 Nations Global 5-minutes soil database.

153 **3.1.2 Model Setup**

154 The WRF model is centred over the Emilia Romagna Region, and integrates three nested
155 domains (D1, D2, D3), with the horizontal spacing of 45 km x 45 km (outer domain, D1), 15
156 km x 15 km (inner domain, D2), and 5 km x 5 km (innermost domain, D3). In this study, the
157 innermost domain D3 is used (88 x 52 grids (west-east and south-north, respectively)), with a
158 two-way nesting scheme considered letting the information from the child domain to be fed
159 back to the parent domain. To drive the WRF model, the European Centre for Medium-Range
160 Weather Forecasts (ECMWF) reanalysis (ERA-Interim) is adopted to provide the study
161 region's boundary and initial conditions. ERA-Interim is a global atmospheric reanalysis that
162 is available from 1979 to 2019 (ERA-5 as a recent update to ERA-Interim may also be used).
163 The spatial resolution of the datasets is approximately 80 km on 60 levels in the vertical from
164 the surface up to 0.1 hPa. It contains 6-hourly gridded estimates of three-dimensional
165 meteorological variables, and 3-hourly estimates of a large number of surface parameters and
166 other two-dimensional fields. Please see (Berrisford et al., 2011) for a detailed documentation of
167 the ERA-Interim.

168 After the initialization, the model needs to be spun-up to derive a physical valid state (e.g.,
169 equilibrium state) (Cai et al., 2014; Cai, 2015). In this study, WRF is spun-up by running through
170 the whole year of 2005. After the spin-up, the WRF model is run in daily timestep from January
171 1, 2006, to December 31, 2015, using the ERA-Interim datasets. The modelled WRF grids
172 within the Emilia Romagna catchment (total of 828 grids) are shown in Figure 2 as black dots,
173 with the elevation map also illustrated in the background.

174 **3.2 Soil Moisture Network Design**



175 For the soil moisture network design, two main problems need to be tackled. First is how many
176 soil moisture sensors are needed within a catchment, and the second is where are the best
177 locations to place them. To solve the first problem, the PCA is used to obtain the optimal
178 number of soil moisture sensors through a threshold analysis. And for the second problem, the
179 *K*-means CA is adopted to determine the locations for the sensor placements.

180 3.2.1. Principal Component Analysis (PCA)

181 When soil moisture data are collected from p soil moisture sensors, these data are often
182 correlated. This correlation reflects the complexity of the catchment and indicates that some of
183 the information collected from one sensor is also contained in the remaining $p-1$ sensors
184 (Gangopadhyay et al., 2001). The role of the PCA is to examine the redundancy of the WRF soil
185 moisture network, and more importantly to highlight the grids that provide the most significant
186 contribution to the principal components (Dai et al., 2017). The optimal number of sensors is
187 dependent on the amount of original variance the network should retain. PCA is a statistical
188 procedure for multivariate feature extraction. It adopts an orthogonal transformation to
189 convert a set of possibly correlated observations into a set of linearly uncorrelated variables
190 called principal components. This transformation is defined in such a way that the first principal
191 component has the largest possible variance, and each succeeding component in order has the
192 highest variance possible under the constraint that it is orthogonal to the preceding components
193 (Wold et al., 1987).

194 In this study, we have p WRF soil moisture grids with N observations (the time series of the
195 data, i.e., 10-year daily datasets). The covariance matrix $p \times p$ can be calculated which is
196 denoted as X , and the eigenvectors and the eigenvalues of the matrix can also be determined,
197 correspondingly. Since the eigenvectors of the X are orthogonal, the p eigenvectors are used to
198 construct the principal components, which can be represented as:



224 Because the optimal number of clusters (k) has already been determined by the PCA, k -means
225 clustering method is utilised in this study to divide the original p datasets into k clusters. k -
226 means approach is a typical distance-based clustering method which uses the distance as the
227 indicator for similarity among objects (i.e., the smaller the distance, the higher the similarity
228 of two objects) (Kodinariya and Makwana, 2013). In this study, the Euclidean distance is adopted
229 as the distance measurement. It is a simple and widely used way of calculating the distances
230 between objects in a multidimensional space (Danielsson, 1980). The centroid of each cluster is
231 the point which the sum of Euclidean distances from all objects in that cluster is minimized. It
232 is an iterative approach repeated for all of the clusters. Since an initial set of cluster centres is
233 needed to be given for the CA to start, the resultant performance will be sensitive to the initial
234 setting. In order to obtain an efficient performance, the WRF grids are ordered by their long-
235 term mean soil moisture and the initial cluster centres are selected evenly from the new
236 sequence (based on the number of k from the PCA). After which, the WRF grids are attributed
237 to the closest cluster accordingly.

238

239 Within each of the optimised clusters, we propose two ways to find the most suitable grid for
240 the sensor placement. One way is by finding the grid which gives the median averaged soil
241 moisture in each of the cluster (denoted as CA-Med), and another is through identifying the
242 maximum averaged soil moisture in each of the cluster (denoted as CA-Max) (Dai et al., 2017).
243 As a result, for each cluster, there is one optimal grid, and grouped with the other optimal grids
244 found in other clusters, the ideal placements for the soil moisture sensors are identified. The
245 group of the selected grids is considered to be the optimal combination of locations that can
246 provide the desired variance of the original WRF soil moisture measurements over the whole
247 catchment.

248 3.3 Network Evaluation



249 Since there is no existing optimal in-situ soil moisture network that can be used as a reference
250 for the evaluation, it is challenging to assess the designed network performance based on a
251 comparison study. However, the designed network should be efficient enough to represent the
252 maximum amount of information with the minimum number of sensors within a catchment. In
253 other words, the designed network should retain **the main catchment-scale soil moisture**
254 **information** of the original WRF network, which is particularly important for the hydrological
255 modelling. To assess the network in such an aspect, the soil moisture information contained by
256 the designed and the original network are compared. Two statistical indicators are used for the
257 purpose, namely the Pearson correlation coefficient and the Nash–Sutcliffe coefficient.

258 The Pearson correlation coefficient (r) is a statistical measure of the linear correlation between
259 two sets of datasets, which in this study can estimate the ~~systematic deviation~~ between the
260 designed (R_d) and the original (R_o) catchment-scale soil moisture variations, and it is calculated
261 by the following equation:

$$262 \quad r_{R_o, R_d} = \frac{E[R_d R_o] - E[R_d]E[R_o]}{\sqrt{(E[R_d^2] - E[R_d]^2) \times (E[R_o^2] - E[R_o]^2)}} \quad (3)$$

263 where E is the mean value of the corresponding vector. In this study, the optimal performance
264 is achieved when r_{R_o, R_d} equals to 1

265 Nash-Sutcliffe Efficiency (NSE) (Nash and Sutcliffe, 1970) is used widely in hydrology to
266 evaluate the prediction accuracy in hydrological modelling, which can be obtained by:

$$267 \quad NSE = 1 - \frac{\sum(R_o^t - R_d^t)^2}{\sum(R_o^t - E[R_o])^2} \quad (4)$$

268 where t is the time-step of the dataset. The NSE ranges $[1, -\infty)$. The closer NSE is to 1, the more
269 accurate the designed network is.

270 **4. Results**



271 4.1. Soil Moisture Network Redundancy Analysis

272 Within the study area of 22,124 km², there is a total number of 828 WRF soil moisture grids.
273 With such a dense network, there should exist information redundancy. To explore this, a cross-
274 correlation (r) matrix for all of the grids over the whole study period is plotted in Figure 3. It
275 can be seen that the majority part of the map is in blue-tone, which means most of the grids
276 (85%) are correlated ($r > 0.5$) with the others (as shown in Table 2). In addition, over half of
277 the grids (52%) have high correlation ($r > 0.8$) with the rest of the grids; and even 15% of the
278 grids can achieve very high correlation ($r > 0.9$). However, it is clear from the map some grids
279 (e.g., grid number 396-398, 523-529) are more heterogeneous than the others (red-tone, with
280 low correlation < 0.3 observed), which means more soil moisture sensors might need to be
281 installed in those locations. The catchment map with the indicated WRF grid numbers is
282 presented in Figure 4a). A further exploration of cross-correlation performance using box plots
283 is shown in Figure 4b). The locations of the selected grids (as in Figure 4b) are marked in
284 Figure 4a) with red circles. It can be seen the nine grids are distributed evenly within the
285 catchment in order to represent a spectrum of catchment features (e.g., different land covers,
286 elevations, soil types etc.). From the box plot, it can be seen for a specific grid, the cross-
287 correlation can range from as low as below 0.1 to as high as almost 1. The large range is
288 particularly obvious for Grid 500, which is located at the plain zone near the east boundary of
289 the catchment and is close to the Valli di Comacchio lagoon. The closeness to the waterbody
290 could mean its soil moisture is dominated more by the waterbody than by the local weather
291 conditions, in comparison with grids located further away. For Grid 100, its correlation with
292 the rest of the grids in the catchment is relatively low, with 75% percentile of the cross-
293 correlations less than 0.6. The potential reason could be because it is located in the southern
294 mountainous zone, with high-density of tree coverage and complex topographic conditions, its
295 soil moisture is more heterogeneous than the other grids. A similar condition is observed for



296 Grid 1 which is also located in a hilly zone in the southern boundary of the catchment (i.e.,
297 lower correlation as shown in the boxplots). Such a phenomenon is not unexpected and could
298 mean more sensors are needed in those complex zones for better soil moisture monitoring
299 purpose. However, for Grids like 300, and 600 (and the surrounding areas), since the majority
300 of their correlations are high and they are located in plain areas with no water boundary nearby,
301 they could be arranged with a smaller number of soil moisture sensors.

302 **4.2. Soil Moisture Sensor Number**

303 In summary, through the cross-correlation exploration, many parts of the WRF soil moisture
304 ~~network~~ are significantly redundant, whilst for some parts, a denser network is indeed needed.
305 To systematically investigate the redundancy degree of the network, the PCA approach is
306 applied. Figure 5a) shows the PCA results to provide useful guidance on the acceptable loss of
307 information. It is clear to see the first principal component carries close to 80% of the total
308 variance, with the second component bringing this to nearly 90%. This result again indicates
309 the high redundancy exists in the ~~network~~, and just one component can contain almost 80% of
310 the total soil moisture information. To better understand the relationship between the principal
311 component numbers, the variance contribution rate, as well as the corresponding required grids
312 number, a set of variance contribution rates from 70% to 97.5% is used as the representatives.
313 The required number of components and the grids are listed accordingly in Table 3. It can be
314 seen only one component with 6 grids is sufficient to retain 70% of the soil moisture
315 information. Even when the variance is set at 80%, only two components are needed to meet
316 the requirement, and the corresponding number of soil moisture grids is 11 (1.3% percent of
317 the total grids). To satisfy 90% variance, three components are needed, and although the total
318 number of grids is increased to 50, it is still significantly less than the WRF's full inputs. The
319 detailed numbers further indicate the relatively high level of redundancy in the WRF's original
320 ~~soil moisture network~~.



321 The trend can also be observed through the Elbow curve which is illustrated in Figure 5b). It
322 presents the relationship between the variance and the number of grids. It can be seen to meet
323 the increment of variance, the required number of grids also increases. But the growth rate is
324 the most significant when the variance is smaller than 70% and then slows down gradually
325 after that. When the variance meets 95%, the rate is further weakened. Based on the curve, it
326 is suggested the desired variance (i.e., trade-off point) between 80% and 95%. The required
327 number of soil moisture grids for 80%, 85%, 90%, and 95% is 11, 21, 50, and 184 respectively.
328 It is clear, in order to achieve the 95% variance, a significantly greater number of additional
329 grids are required, that is 268% more than for the 90% variance case. Therefore, for further
330 improvement of variance from 90% to 95%, the economic cost for the additional number of
331 sensors might not be as valuable as for the 85% to 90% case (138% additional sensors are
332 required for the enhancement).

333 **4.3. Soil Moisture Sensor Location Design**

334 Once the degree of redundancy for the full WRF soil moisture network is established, the next
335 step is to determine the optimal locations for sensor placements. Because the components from
336 the PCA do not directly represent the physical WRF grids, cluster analysis is thus carried out
337 to identify the specific grid locations. Here, CA-Max and CA-Med are used. The designed
338 networks for CA-Max and CA-Med are illustrated in **Figure 6 and 7**, respectively. The
339 indicated locations in the figures provide guidance on the preferential areas for the soil moisture
340 sensor placements. Each of the methods gives a different set of sensor locations, for instance,
341 the selected optimal soil moisture grids from the CA-Max method tend to be located at the
342 catchment boundary, and the situation is particularly obvious for the low variance cases (i.e.,
343 70% - 80%). For example, when the variance is set at 70%, the selected optimal locations from
344 the CA-Max is mostly distributed near the catchment's southern boundary, while from the CA-
345 Med, it is more homogeneously distributed (i.e., one at the southern boundary, one at the north,



346 two at the north-western part, and two at the north-eastern part). When the variance is increased,
347 for instance at 90%, the difference between the two CA methods becomes less distinctive.
348 Despite this, it can still be seen for the CA-Max, there is less coverage of sensors at the western
349 and the eastern parts of the catchment, with most of the sensors located at the mid-region.
350 However, for the same variance, the sensor distribution from the CA-Med looks more evenly
351 distributed visually. Nevertheless, when the variance reaches as high as 97.5%, the difference
352 from the two methods becomes rather small, as 367 sensors are located covering most parts of
353 the catchment in both cases.

354 4.4. Soil Moisture Network Evaluation

355 The evaluation of the designed network is challenging, as there are no standard assessment
356 criteria available to guide on what kind of network is the most appropriate for a given study
357 area. In essence, the designed network should be efficient, which means the network should
358 contain the maximum amount of information with a minimal number of sensors. In this study
359 since we focus on the soil moisture's hydrological applications (catchment-scale), to evaluate
360 the efficiency of the proposed schemes, the catchment-scale soil moisture data derived by the
361 designed networks are compared with the WRF's full inputs (828 grids). Both the areal spatial
362 mean and standard deviation are calculated. The Pearson correlation coefficient and the Nash–
363 Sutcliffe coefficient are used to quantify the relationships between the two soil moisture
364 datasets. The results for both the CA-Med and the CA-Max are compared in Figure 8. Based
365 on the areal mean soil moisture (Figure 8 a) and c)), it is clear to see the CA-Med outperforms
366 the CA-Max for the majority of the variance cases (both *NSE* and *r*), except for the *NSE* results
367 when the variance is over 90%. Moreover, for the *NSE* results, a decline of the performance
368 can be observed clearly after it passes the 90% variance point, which illustrates that an
369 increment of sensor number does not necessarily mean a rise of the performance. For the
370 standard deviation, the disparity between the two methods is smaller. When the variance is



371 below 80%, the growth trend for the CA-Med case is not clear, as it firstly drops at the 75%
372 point and then climbs up again when the variance increases. Whereas for the CA-Max case,
373 there is a clear upward trend. Similar to Figure 8 a), it is interesting to see for the areal standard
374 deviation in Figure 8 b) and d), the *NSE* and *r* also start to drop after reaching around 90%,
375 which again indicates the increment of sensor number does not positively link to the
376 improvement of network performance (here in the aspect of spatial variation). The evaluation
377 results are summarised in Table 4 for numerical comparison. Since CA-Med surpasses CA-
378 Max for most of the cases, it is chosen for the network design. In the aspect of the desired
379 variance, because as discussed earlier, when the variance climbs over 90%, the performance
380 instead drops. Therefore 90% variance is suitable to be used for the network design in this case.

381 The time series plots of the areal soil moisture mean and standard deviation are shown in Figure
382 9. Generally, the designed network can estimate the catchment's mean soil moisture very well,
383 as it follows the variation of the WRF's full input dataset closely (*NSE* = 0.995 and *r* = 0.999).
384 For the standard deviation, the general trend from both datasets shows a higher spatial variation
385 of soil moisture over the dry season and lower variation during the wet season. The spatial
386 variation is averaged around 0.04 m³/m³ throughout the whole study period. However, there
387 are some disparities between the two datasets, in particular, during the wet season (bottom
388 peaks in the STD plot), the designed network at several occasions overestimates the spatial soil
389 moisture variation, and during the dry season (top peaks in the STD plot), it underestimates
390 instead. Nevertheless, the differences are small and the correlation between the two datasets is
391 high, with *NSE* = 0.973 and *r* = 0.990 obtained. In conclusion, the designed network can
392 maintain the dominated information of the WRF's full-grid input well.

393 The sensor displacements for the designed and the existing (in-situ) networks are illustrated in
394 Figure 10. In comparison with the distribution of the proposed network, the existing network
395 is clearly biased, with all of the sensors located in the mid-plain zone only. Such distribution



396 (i.e., no sensors located at the southern mountainous (highly-vegetated) region) can have
397 adverse impacts on the accuracy of the areal mean soil moisture estimation. Scatterplots of the
398 areal mean soil moisture calculated from the designed and the existing networks are also
399 presented in Figure 11. The performance difference between the two networks is clear to
400 observe. For the proposed network, the points are located close to the identical line, whereas
401 for the existing network, due to the inappropriate sensor distributions over the catchment, the
402 points are more dispersive ($NSE = 0.889$). The performance of the existing network in
403 comparison with the proposed networks indicates that it cannot retain even 70% of the variance
404 (as compared with the NSE results in Table 4), as the NSE for the 70% CA-Med can achieve
405 0.949. For the existing network, without putting sensors in the highly vegetated region, the
406 network clearly underestimates soil moisture variations during the dry season (i.e., for the cases
407 when the soil moisture is less than $0.25 \text{ m}^3/\text{m}^3$)

408 5. Discussions and conclusions

409 With the low-cost soil moisture sensors becoming more and more available and modern
410 communication technology (i.e., Internet of Things), it is expected more in-situ soil moisture
411 sensors will be installed in the future. However, unlike the rich literature in the rain gauge
412 network design field, there is a research gap in soil moisture network design for catchment-
413 scale applications. As a result, research is urgently needed to fill this important knowledge gap.
414 ~~As one of the pioneering studies in this field,~~ a low-data requirement method is proposed in
415 this study for the in-situ soil moisture network design. Through a series of evaluations of the
416 developed network, it can be concluded that the method can provide efficient catchment-scale
417 soil moisture estimations (i.e., high accuracy of the areal mean and standard deviation soil
418 moisture estimations). To retain 90% variance, a total of 50 sensors in a $22,124 \text{ km}^2$ catchment
419 is needed. In comparison with the original number of WRF's grids (828 grids), the proposed
420 network requires significantly smaller number of sensors. Furthermore, in comparison with the



421 existing soil moisture network in the Emilia Romagna region, the proposed network has sensors
422 more evenly distributed, covering most representative parts of the catchment (e.g., both plain
423 and mountainous regions), and can obtain more accurate catchment-scale soil moisture
424 estimation. However, there are several points need to be discussed as follows.

425 The first point is about the uncertainty of the WRF's soil moisture estimations, which could
426 influence the accuracy of the network design. It is acknowledged that the reliability of the
427 designed network is influenced by the performance of the WRF model. To evaluate the WRF
428 results and test whether the proposed network can produce the catchment-scale soil moisture
429 well, a long-term densely covered soil moisture network will be required. Setting up such a
430 network is challenging and difficult to realise due to the high installation and maintenance cost.
431 In this study, a long-term WRF soil moisture estimation with 1-year spin-up time is used which
432 could to some extent produce a more stable result. But since "all models are wrong" (by George
433 E. P. Box), an uncertainty model (Zhuo et al., 2016) could be proposed to be integrated with the
434 network design scheme. For example, we can generate a large number of probable "true soil
435 moisture" datasets based on the proposed uncertainty model so that a set of possible soil
436 moisture networks can be produced. As a result, the designed network will be expressed in a
437 probabilistic form instead of a determinate form. In addition, a decision-making scheme
438 considering different conditions (e.g., accessibility, installation and maintenance cost) under
439 the uncertainty can be developed to select the most suitable soil moisture network. The
440 uncertainty influence of the WRF soil moisture on the network design will be investigated in
441 future studies.

442 Second, the case study is based on the daily soil moisture inputs for the hydrological
443 applications. With different research needs (meteorology, climatology, hydrology, water
444 resources, geology, etc.), various temporal-scale of soil moisture data might be required, for
445 example, climate change study requires soil moisture data in decades or hundreds of years



446 which often needs annual-scale measurements; drought assessment requires monthly to
447 seasonal datasets; while for hydrometeorological prediction applications, hourly datasets might
448 be needed. For the network design, the input data's temporal scale (daily, weekly, monthly,
449 yearly) can influence the final network design, therefore it is worth investigating in future
450 studies about the temporal-scale effect on the network design.

451 Third, for a complex catchment like Emilia Romagna, other uncertainty sources apart from the
452 WRF model can also affect the performance of the designed network; for instance, the study
453 area has varied climate conditions (a mixture of subcontinental and cool temperate) and distinct
454 seasonal changes (wet/dry seasons). Therefore separating/combining networks under different
455 catchment conditions could result in an improved soil moisture network design. Furthermore,
456 the poor accessibility to sensors is another challenging point that can hamper the performance
457 of the designed network in real life, for instance, even an in-situ network follows tightly
458 through a systematic design scheme, without proper maintenance due to the accessibility issue,
459 the quality of the retrieved data can be highly affected. Therefore, the accessibility factor
460 should also be considered for the network design (e.g., can be considered during the CA for
461 the sensor placements).

462 Since the forcing data for the WRF model is globally covered, the proposed scheme can largely
463 benefit ungauged catchments. On the other hand, in places where dense soil moisture networks
464 are already available, the proposed scheme could also help in minimizing the cost by reducing
465 the number of sensors. Another advantage of the method is that the number of soil moisture
466 sensors can be changed based on different variances to meet various requirements. Through
467 selecting different variance levels, the redundancy of the WRF's full-input network can be
468 assessed, and the corresponding optimal sensor number can be determined. However, the
469 proposed scheme is still in its infancy with a lot of refinements and further explorations needed,



470 therefore it is hoped this paper will stimulate more studies by the community in tackling the
471 soil moisture network design problem.

472 **Acknowledgement**

473 This research is supported by the National Natural Science Foundation of China (NSFC, grant
474 no. 41871299), and Resilient Economy and Society by Integrated SysTems modelling
475 (RESIST), Newton Fund via Natural Environment Research Council (NERC) and Economic
476 and Social Research Council (ESRC) (NE/N012143/1).

477 **References**

478 Adhikary, S. K., Yilmaz, A. G., and Muttill, N.: Optimal design of rain gauge network in the
479 Middle Yarra River catchment, Australia, *Hydrol. Process.*, 29, 2582-2599, 2015.

480 Albergel, C., De Rosnay, P., Gruhier, C., Muñoz-Sabater, J., Hasenauer, S., Isaksen, L., Kerr,
481 Y., and Wagner, W.: Evaluation of remotely sensed and modelled soil moisture products using
482 global ground-based in situ observations, *Remote Sens. Environ.*, 118, 215-226, 2012.

483 Bayat, B., Hosseini, K., Nasser, M., and Karami, H.: Challenge of rainfall network design
484 considering spatial versus spatiotemporal variations, *J. Hydrol.*, 574, 990-1002, 2019.

485 Berrisford, P., Dee, D., Poli, P., Brugge, R., Fielding, K., Fuentes, M., Kallberg, P., Kobayashi,
486 S., Uppala, S., and Simmons, A.: The ERA-Interim archive, version 2.0,
487 <https://www.ecmwf.int/node/8174>, 2011.

488 Bontemps, S., Defourny, P., Radoux, J., Van Bogaert, E., Lamarche, C., Achard, F., Mayaux,
489 P., Boettcher, M., Brockmann, C., and Kirches, G.: Consistent global land cover maps for
490 climate modelling communities: Current achievements of the ESA's land cover CCI,
491 *Proceedings of the ESA Living Planet Symposium*, Edinburgh, 2013, 9-13,

492 Brocca, L., Ciabatta, L., Massari, C., Camici, S., and Tarpanelli, A.: Soil moisture for
493 hydrological applications: open questions and new opportunities, *Water*, 9, 140, 2017.

494 Cai, X., Yang, Z. L., Xia, Y., Huang, M., Wei, H., Leung, L. R., and Ek, M. B.: Assessment of
495 simulated water balance from Noah, Noah-MP, CLM, and VIC over CONUS using the
496 NLDAS test bed, *J. Geophys. Res. Atmos.*, 119, 7137-7151, 2014.

497 Cai, X.: Hydrological assessment and biogeochemical advancement of the Noah-MP land
498 surface model, Doctor of Philosophy, Geological Sciences, The University of Texas at Austin,
499 164 pp., 2015.



- 500 Chaney, N. W., Roundy, J. K., Herrera-Estrada, J. E., and Wood, E. F.: High-resolution
501 modeling of the spatial heterogeneity of soil moisture: Applications in network design, *Water*
502 *Resour. Res.*, 51, 619-638, 2015.
- 503 Chen, F., and Dudhia, J.: Coupling an advanced land surface-hydrology model with the Penn
504 State-NCAR MM5 modeling system. Part I: Model implementation and sensitivity, *Monthly*
505 *Weather Review*, 129, 569-585, 2001.
- 506 Chen, Y. C., Wei, C., and Yeh, H. C.: Rainfall network design using kriging and entropy,
507 *Hydrol. Process.*, 22, 340-346, 2008.
- 508 Crow, W., Chen, F., Reichle, R., Xia, Y., and Liu, Q.: Exploiting soil moisture, precipitation,
509 and streamflow observations to evaluate soil moisture/runoff coupling in land surface models,
510 *Geophys. Res. Lett.*, 45, 4869-4878, 2018.
- 511 Dai, Q., Bray, M., Zhuo, L., Islam, T., and Han, D.: A scheme for rain gauge network design
512 based on remotely sensed rainfall measurements, *J. Hydrometeorol.*, 18, 363-379, 2017.
- 513 Danielsson, P.-E.: Euclidean distance mapping, *Computer Graphics and Image Processing*, 14,
514 227-248, 1980.
- 515 Dorigo, W., Wagner, W., Albergel, C., Albrecht, F., Balsamo, G., Brocca, L., Chung, D., Ertl,
516 M., Forkel, M., and Gruber, A.: ESA CCI Soil Moisture for improved Earth system
517 understanding: State-of-the art and future directions, *Remote Sens. Environ.*, 203, 185-215,
518 2017.
- 519 Dudhia, J.: Numerical study of convection observed during the winter monsoon experiment
520 using a mesoscale two-dimensional model, *Journal of the Atmospheric Sciences*, 46, 3077-
521 3107, 1989.
- 522 Ek, M., Mitchell, K., Lin, Y., Rogers, E., Grunmann, P., Koren, V., Gayno, G., and Tarpley, J.:
523 Implementation of Noah land surface model advances in the National Centers for
524 Environmental Prediction operational mesoscale Eta model, *J. Geophys. Res. Atmos.*, 108,
525 2003.
- 526 Everitt, B., Landau, S., and Leese, M.: *Cluster Analysis 4th Edition*, Taylor & Francis, London,
527 2001.
- 528 Friesen, J., Rodgers, C., Oguntunde, P. G., Hendrickx, J. M., and van de Giesen, N.: Hydrotopy-
529 based protocol to determine average soil moisture over large areas for satellite calibration and
530 validation with results from an observation campaign in the Volta Basin, West Africa, *IEEE T*
531 *Geosci Remote*, 46, 1995-2004, 2008.
- 532 Fuamba, M., Branger, F., Braud, I., Batchabani, E., Sanzana, P., Sarrazin, B., and Jankowsky,
533 S.: Value of distributed water level and soil moisture data in the evaluation of a distributed
534 hydrological model: Application to the PUMMA model in the Mercier catchment (6.6 km²) in
535 France, *J. Hydrol.*, 569, 753-770, 2019.



- 536 Gangopadhyay, S., Das Gupta, A., and Nachabe, M.: Evaluation of ground water monitoring
537 network by principal component analysis, *Groundwater*, 39, 181-191, 2001.
- 538 Gilliland, E. K., and Rowe, C. M.: A comparison of cumulus parameterization schemes in the
539 WRF model, *Proceedings of the 87th AMS Annual Meeting & 21th Conference on Hydrology*,
540 2007,
- 541 Hong, S.-Y., Noh, Y., and Dudhia, J.: A new vertical diffusion package with an explicit
542 treatment of entrainment processes, *Mon. Weather Rev.*, 134, 2318-2341, 2006a.
- 543 Hong, S.-Y., Noh, Y., and Dudhia, J.: A new vertical diffusion package with an explicit
544 treatment of entrainment processes, *Monthly Weather Review*, 134, 2318-2341, 2006b.
- 545 Jiménez, P. A., Dudhia, J., González-Rouco, J. F., Navarro, J., Montávez, J. P., and García-
546 Bustamante, E.: A revised scheme for the WRF surface layer formulation, *Mon. Weather Rev.*,
547 140, 898-918, 2012a.
- 548 Jiménez, P. A., Dudhia, J., González-Rouco, J. F., Navarro, J., Montávez, J. P., and García-
549 Bustamante, E.: A revised scheme for the WRF surface layer formulation, *Monthly Weather*
550 *Review*, 140, 898-918, 2012b.
- 551 Kain, J. S.: The Kain-Fritsch convective parameterization: An update, *Journal of Applied*
552 *Meteorology*, 43, [http://dx.doi.org/10.1175/1520-0450\(2004\)043<0170:TKCPAU>2.0.CO;2](http://dx.doi.org/10.1175/1520-0450(2004)043<0170:TKCPAU>2.0.CO;2),
553 2004a.
- 554 Kain, J. S.: The Kain-Fritsch convective parameterization: An update, *J. Appl. Meteorol.*, 43,
555 [http://dx.doi.org/10.1175/1520-0450\(2004\)043<0170:TKCPAU>2.0.CO;2](http://dx.doi.org/10.1175/1520-0450(2004)043<0170:TKCPAU>2.0.CO;2), 2004b.
- 556 Kodinariya, T. M., and Makwana, P. R.: Review on determining number of Cluster in K-Means
557 Clustering, *Int. J. Adv. Res. Comput. Sci. Manag. Stud.*, 1, 90-95, 2013.
- 558 Laiolo, P., Gabellani, S., Campo, L., Silvestro, F., Delogu, F., Rudari, R., Pulvirenti, L., Boni,
559 G., Fascetti, F., and Pierdicca, N.: Impact of different satellite soil moisture products on the
560 predictions of a continuous distributed hydrological model, *Int J Appl Earth Obs*, 48, 131-145,
561 2016.
- 562 Lopez, P. L., Wanders, N., Schellekens, J., Renzullo, L. J., Sutanudjaja, E. H., and Bierkens,
563 M. F.: Improved large-scale hydrological modelling through the assimilation of streamflow
564 and downscaled satellite soil moisture observations, *Hydrol. Earth Syst. Sci.*, 20, 3059-3076,
565 2016.
- 566 Mlawer, E. J., Taubman, S. J., Brown, P. D., Iacono, M. J., and Clough, S. A.: Radiative transfer
567 for inhomogeneous atmospheres: RRTM, a validated correlated-k model for the longwave,
568 *Journal of Geophysical Research: Atmospheres*, 102, 16663-16682, 1997.
- 569 Nash, J. E., and Sutcliffe, J. V.: River flow forecasting through conceptual models part I—A
570 discussion of principles, *J. Hydrol.*, 10, 282-290, 1970.
- 571 Weather research and forecasting model, 2018.



- 572 Nistor, M. M.: Spatial distribution of climate indices in the Emilia-Romagna region, *Meteorol.*
573 *Appl.*, 23, 304-313, 2016.
- 574 Pardo-Igúzquiza, E.: Optimal selection of number and location of rainfall gauges for areal
575 rainfall estimation using geostatistics and simulated annealing, *J. Hydrol.*, 210, 206-220, 1998.
- 576 Pistocchi, A., Calzolari, C., Malucelli, F., and Ungaro, F.: Soil sealing and flood risks in the
577 plains of Emilia-Romagna, Italy, *J. Hydrol. Reg. Stud.*, 4, 398-409, 2015.
- 578 Rajib, M. A., Merwade, V., and Yu, Z.: Multi-objective calibration of a hydrologic model using
579 spatially distributed remotely sensed/in-situ soil moisture, *J. Hydrol.*, 536, 192-207, 2016.
- 580 Robock, A., Vinnikov, K. Y., Srinivasan, G., Entin, J. K., Hollinger, S. E., Speranskaya, N. A.,
581 Liu, S., and Namkhai, A.: The global soil moisture data bank, *Bull. Amer. Meteor. Soc.*, 81,
582 1281-1300, 2000.
- 583 Skamarock, W., Klemp, J., Dudhia, J., Gill, D., Barker, D., Duda, M., Huang, X., Wang, W.,
584 and Powers, J.: A description of the advanced research WRF Version 3, NCAR technical note,
585 Mesoscale and Microscale Meteorology Division, National Center for Atmospheric Research,
586 Boulder, Colorado, USA, 2008.
- 587 Skamarock, W. C., Klemp, J. B., Dudhia, J., Gill, D. O., Barker, D. M., Wang, W., and Powers,
588 J. G.: A description of the advanced research WRF version 2, National Center for Atmospheric
589 Research Boulder, Colorado, USA, 2005.
- 590 Srivastava, P. K., Han, D., Rico-Ramirez, M. A., O'Neill, P., Islam, T., Gupta, M., and Dai, Q.:
591 Performance evaluation of WRF-Noah Land surface model estimated soil moisture for
592 hydrological application: Synergistic evaluation using SMOS retrieved soil moisture, *J.*
593 *Hydrol.*, 529, 200-212, 2015.
- 594 Stéfanon, M., Drobinski, P., D'Andrea, F., Lebeaupin-Brossier, C., and Bastin, S.: Soil
595 moisture-temperature feedbacks at meso-scale during summer heat waves over Western
596 Europe, *Clim. Dyn.*, 42, 1309-1324, 2014.
- 597 Thompson, G., Field, P. R., Rasmussen, R. M., and Hall, W. D.: Explicit forecasts of winter
598 precipitation using an improved bulk microphysics scheme. Part II: Implementation of a new
599 snow parameterization, *Monthly Weather Review*, 136, 5095-5115, 2008.
- 600 Uber, M., Vandervaere, J.-P., Zin, I., Braud, I., Heisterman, M., Legouët, C., Molinié, G., and
601 Nord, G.: How does initial soil moisture influence the hydrological response? A case study
602 from southern France, *Hydrol. Earth Syst. Sci.*, 22, 6127-6146, 2018.
- 603 Vereecken, H., Huisman, J., Bogena, H., Vanderborght, J., Vrugt, J., and Hopmans, J. W.: On
604 the value of soil moisture measurements in vadose zone hydrology: A review, *Water Resour.*
605 *Res.*, 44, 2008.
- 606 Western, A. W., Zhou, S.-L., Grayson, R. B., McMahon, T. A., Blöschl, G., and Wilson, D. J.:
607 Spatial correlation of soil moisture in small catchments and its relationship to dominant spatial
608 hydrological processes, *J. Hydrol.*, 286, 113-134, 2004.



- 609 Wold, S., Esbensen, K., and Geladi, P.: Principal component analysis, *Chemometr Intell Lab*
610 *Syst* 2, 37-52, 1987.
- 611 Zaidi, S. M., and Gisen, J. I. A.: Evaluation of Weather Research and Forecasting (WRF)
612 Microphysics single moment class-3 and class-6 in Precipitation Forecast, *MATEC Web of*
613 *Conferences*, 2018, 03007,
- 614 Zaitchik, B. F., Santanello, J. A., Kumar, S. V., and Peters-Lidard, C. D.: Representation of
615 soil moisture feedbacks during drought in NASA unified WRF (NU-WRF), *J. Hydrometeorol.*,
616 14, 360-367, 2013.
- 617 Zhuo, L., Dai, Q., Islam, T., and Han, D.: Error distribution modelling of satellite soil moisture
618 measurements for hydrological applications, *Hydrol. Process.*, 30, 2223-2236, 2016.
- 619 Zhuo, L., and Han, D.: Multi-source hydrological soil moisture state estimation using data
620 fusion optimisation, *Hydrol. Earth Syst. Sci.*, 21, 3267-3285, 2017.
- 621 Zhuo, L., Dai, Q., Han, D., Chen, N., and Zhao, B.: Assessment of simulated soil moisture
622 from WRF Noah, Noah-MP, and CLM land surface schemes for landslide hazard application,
623 *Hydrol. Earth Syst. Sci.*, 23, 4199-4218, 2019a.
- 624 Zhuo, L., Dai, Q., Han, D., Chen, N., Zhao, B., and Berti, M.: Evaluation of Remotely Sensed
625 Soil Moisture for Landslide Hazard Assessment, *IEEE J-STARS*, 12, 162-173, 2019b.
- 626 Zwieback, S., Westermann, S., Langer, M., Boike, J., Marsh, P., and Berg, A.: Improving
627 permafrost modeling by assimilating remotely sensed soil moisture, *Water Resour. Res.*, 55,
628 1814-1832, 2019.
- 629
- 630



631 **Table 1.** WRF parameterizations used in this study.

	Settings/ Parameterizations	References
Map projection	Lambert	
Central point of domain	Latitude: 44.54; Longitude: 11.02	
Latitudinal grid length	5 km	
Longitudinal grid length	5 km	
Model output time step	Daily	
Nesting	Two-way	
Land surface model	Noah-MP	
Simulation period	1/1/2006 – 31/12/2015	
Spin-up period	1/1/2005 – 31/12/2005	
Microphysics	New Thompson	(Thompson et al., 2008)
Shortwave radiation	Dudhia scheme	(Dudhia, 1989)
Longwave radiation	Rapid Radiative Transfer Model	(Mlawer et al., 1997)
Surface layer	Revised MM5	(Jiménez et al., 2012b; Chen and Dudhia, 2001)
Planetary boundary layer	Yonsei University method	(Hong et al., 2006b)
Cumulus Parameterization	Kain-Fritsch (new Eta) scheme	(Kain, 2004a)

632

633



634 **Table 2.** The relationship between the percentage of grids, and the cross-correlation.

Cross-correlation (r)	Percentage of grids (%)
0.5	85
0.6	78
0.7	70
0.8	52
0.9	15
0.95	3

635



636 **Table 3.** The number of components and grids to reach % variance threshold (based on the
637 PCA method and the Elbow curve method).

Variance (%)	Components	Number of grids
70.0	1	6
75.0	1	7
80.0	2	11
85.0	2	21
90.0	3	50
92.5	3	94
95.0	3	184
97.5	3	367

638

639

640

641



642 **Table 4.** *NSE* and correlation *r* performance of CA_Med and CA_Max.

Variance	CA_Max_Mean		CA_Med_Mean		CA_Max_STD		CA_Med_STD	
	NSE	r	NSE	r	NSE	r	NSE	r
70.0	0.831	0.978	0.949	0.985	0.601	0.834	0.716	0.876
75.0	0.851	0.984	0.978	0.993	0.778	0.887	0.746	0.870
80.0	0.894	0.990	0.991	0.996	0.867	0.945	0.901	0.951
85.0	0.976	0.997	0.991	0.998	0.926	0.967	0.930	0.976
90.0	0.988	0.998	0.995	0.999	0.963	0.986	0.973	0.990
92.5	0.997	0.998	0.990	0.999	0.969	0.989	0.960	0.992
95.0	0.994	0.999	0.985	0.999	0.932	0.990	0.914	0.986
97.5	0.988	1.000	0.983	1.000	0.910	0.986	0.895	0.982

643

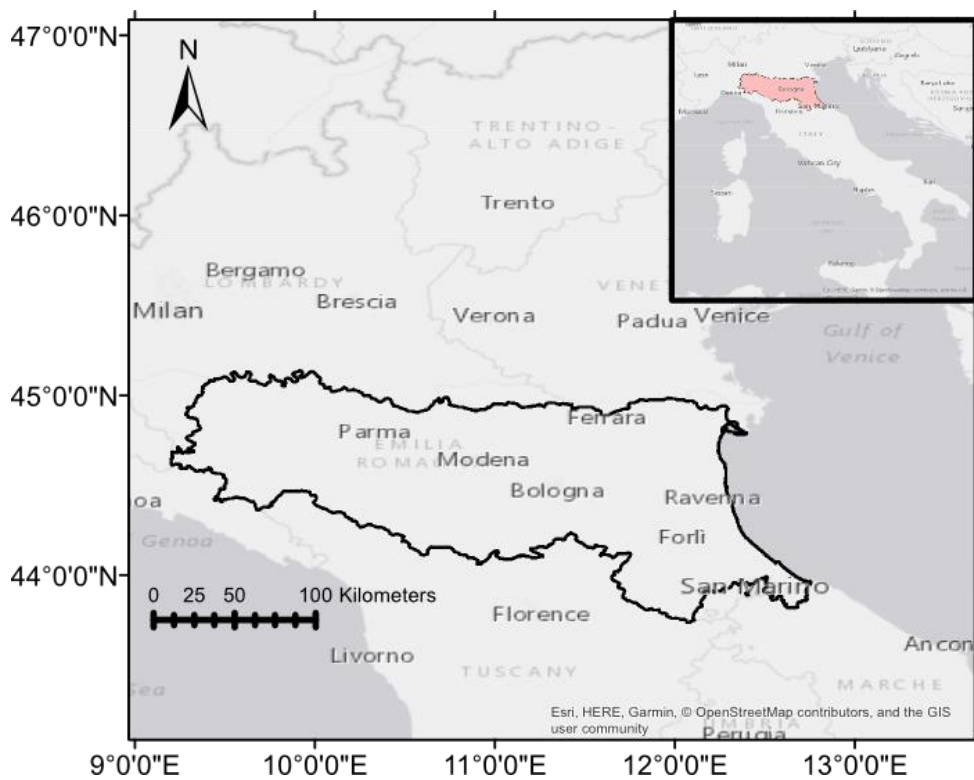
644

645

646

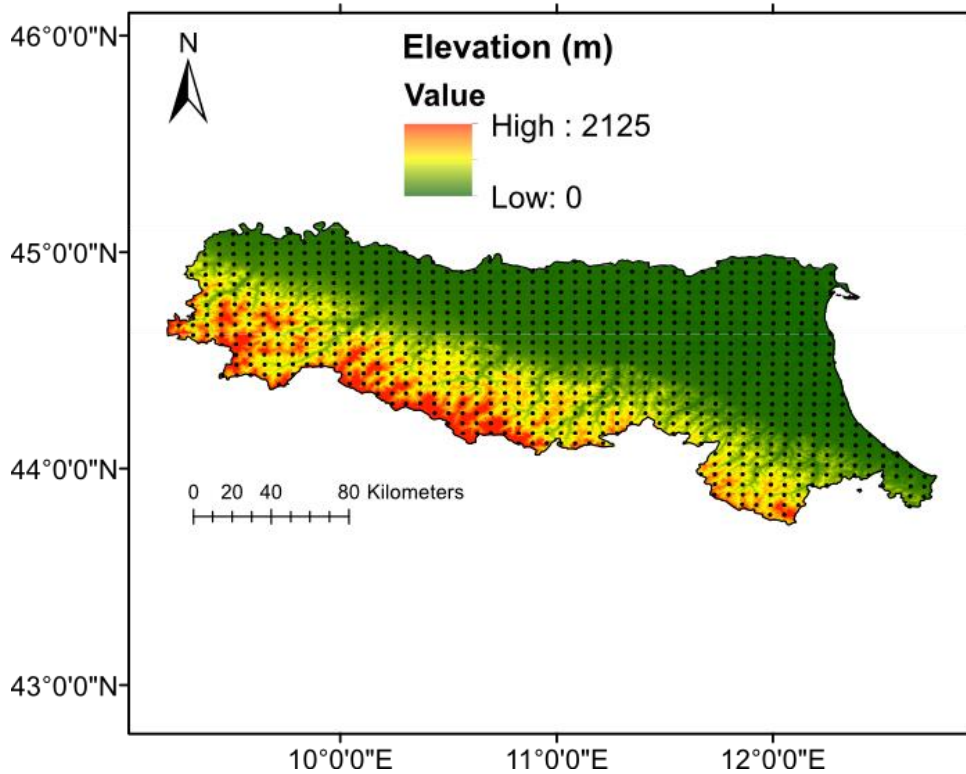
647

648



649

650 **Figure 1.** The geographical map of the Emilia Romagna region.

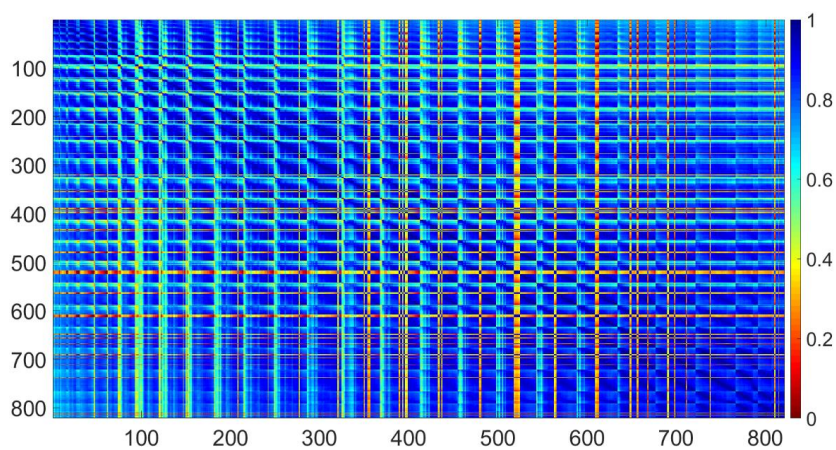


651

652

653 **Figure 2.** WRF grids used in the analysis, with DEM map in the background.

654

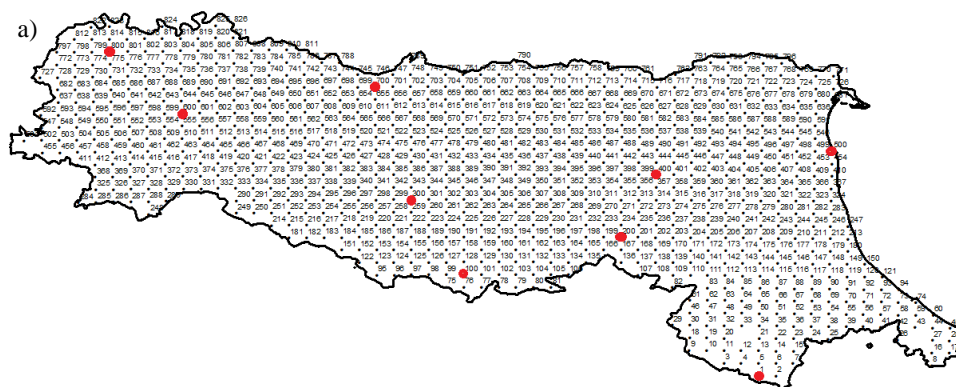


655

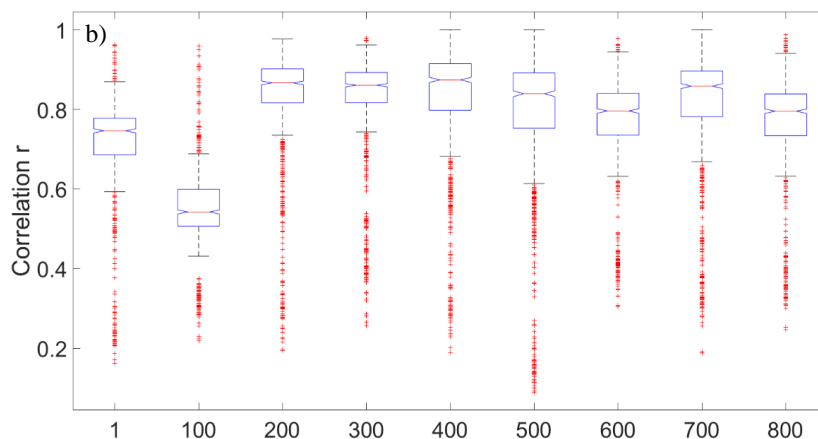
656 **Figure 3.** Cross correlation matrix for the whole catchment.

657

658



659



660

661 **Figure 4.** a) WRF grid number; b) correlation boxplot for the selected grids as highlighted in
662 red in a). For the boxplot, it shows the minimum, maximum, 0.25, 0.50, and 0.75 percentiles
663 and outliers (red cross).

664

665

666

667

668

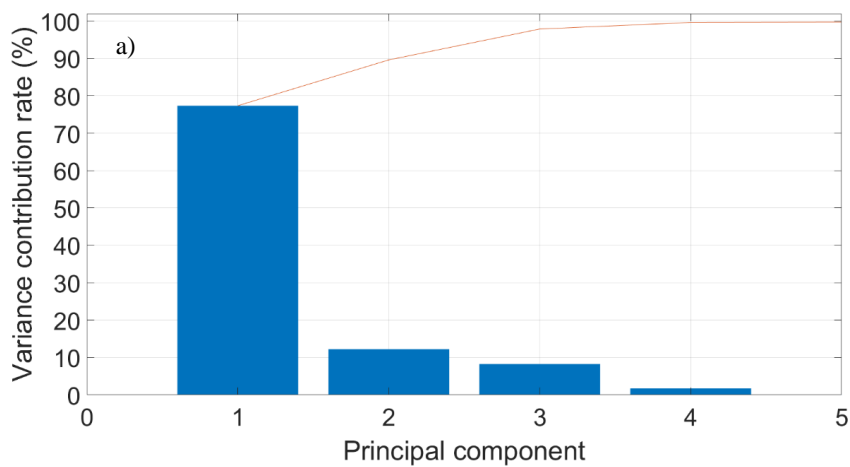
669

670

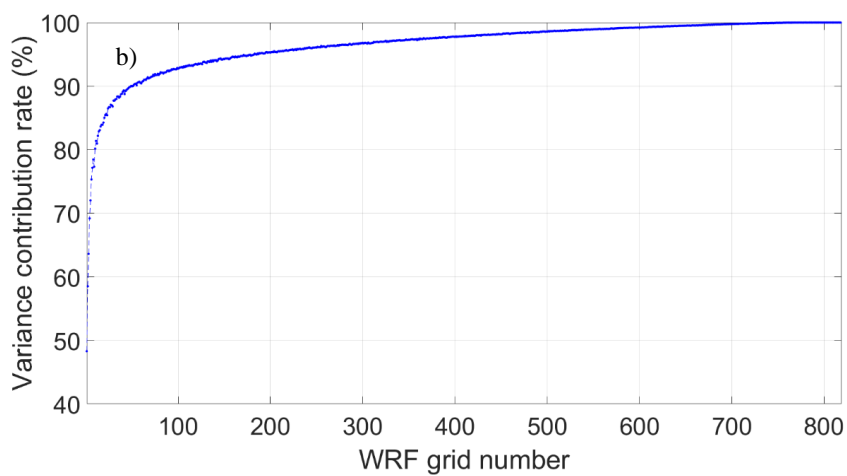
671

672

673



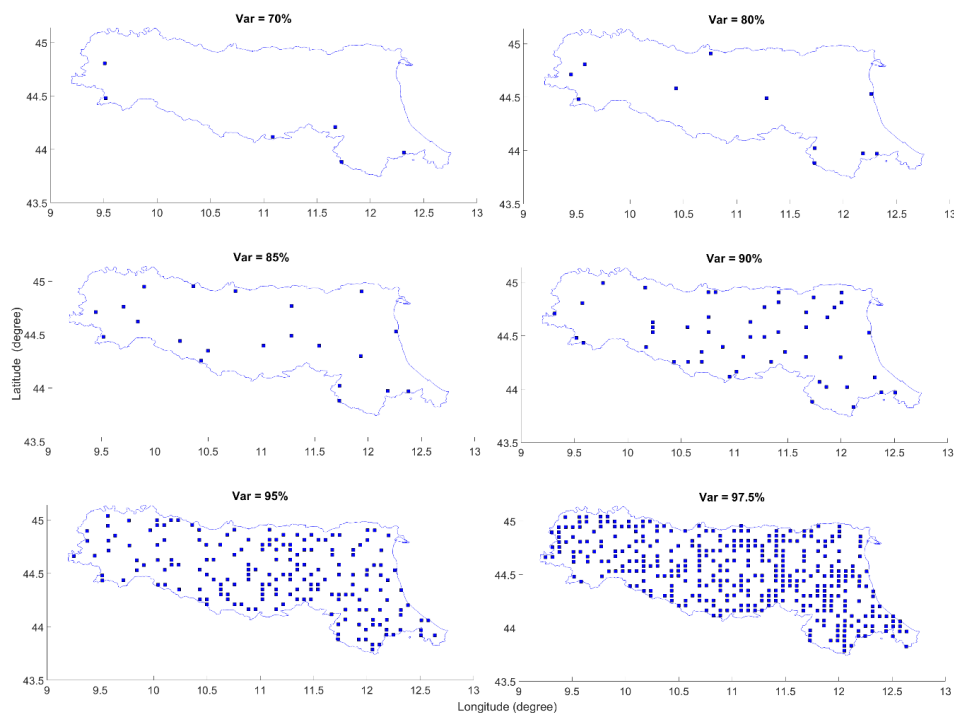
674



675

676 **Figure 5.** a) PCA analysis; b) Elbow curve.

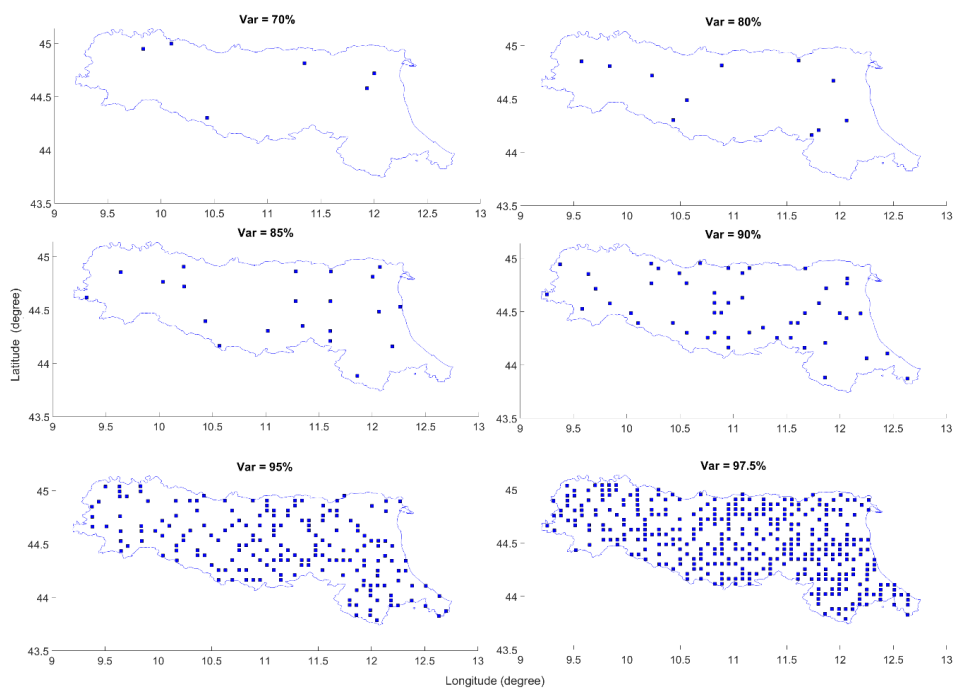
677



678

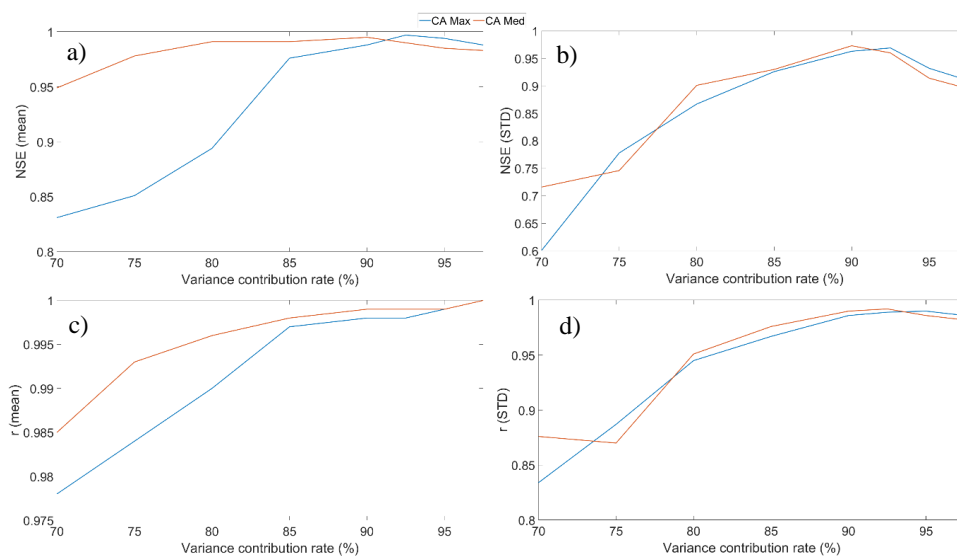
679 **Figure 6.** Designed soil moisture sensor locations, based on CA-Max.

680



681

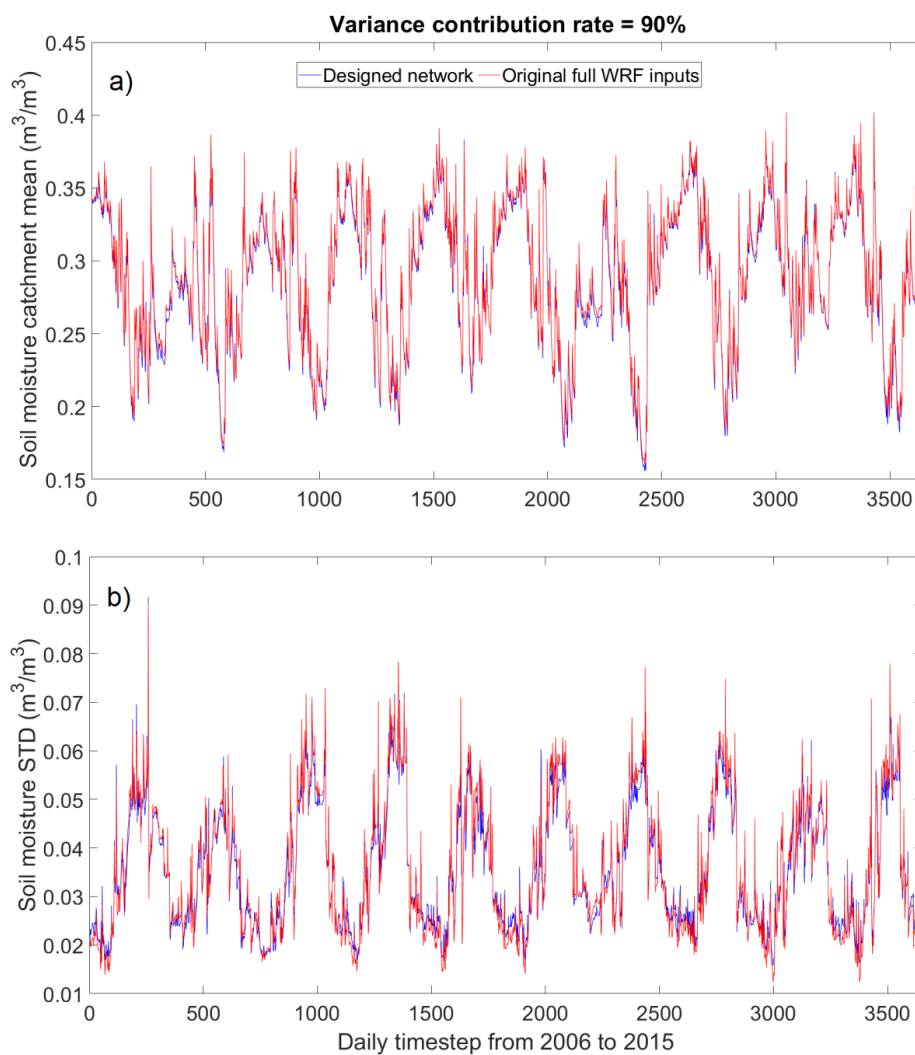
682 **Figure 7.** Designed soil moisture sensor locations, based on CA-Med.



683

684 **Figure 8.** *NSE* and *r* plots: a) *NSE* performance based on the areal mean soil moisture, b) *NSE*
685 performance based on the areal standard deviation soil moisture (STD), c) *r* performance based
686 on the areal mean soil moisture, d) *r* performance based on the areal standard deviation soil
687 moisture.

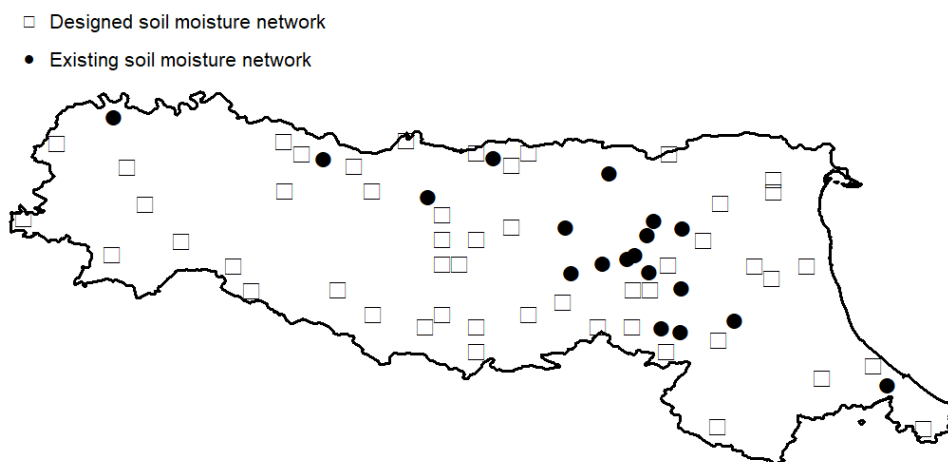
688



689

690 **Figure 9.** a) The areal mean soil moisture of the designed and the WRF's full-input networks,
691 b) the areal soil moisture standard deviation of the designed and the WRF's full-input networks.

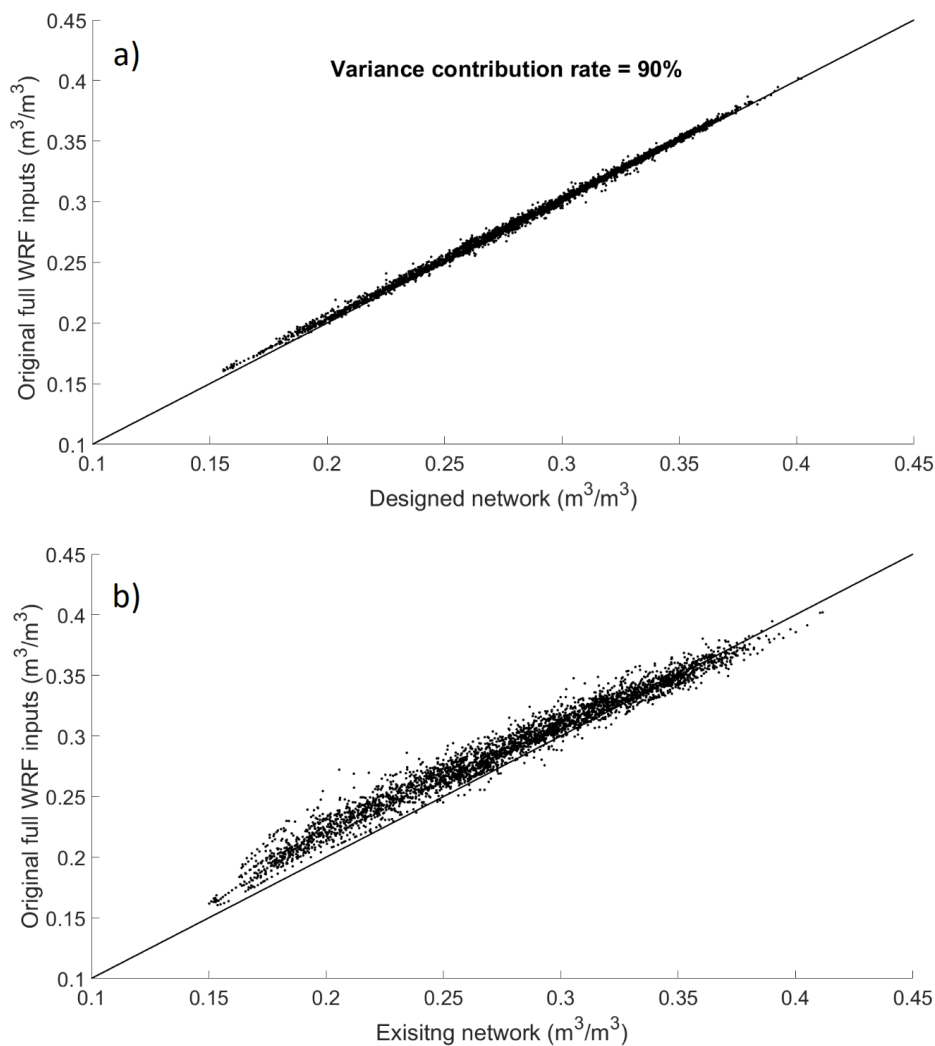
692



693

694 **Figure 10.** Comparison between the existing and the designed soil moisture networks.

695



696

697 **Figure 11.** Scatterplots for areal mean soil moisture: a) WRF full grid inputs against the
698 proposed network ($NSE = 0.995$, $r = 0.998$); b) WRF full grid inputs against the existing in-
699 situ network ($NSE = 0.889$, $r = 0.987$).

700

701

702